Characterization of Histidine Coordination in VO^{2+}-Substituted D-Xylose Isomerase by Orientationally-Selected Electron Spin-Echo Envelope Modulation Spectroscopy

Sergei A. Dikanov,*,†,‡,§ Alexei M. Tyryshkin,† Jürgen Hüttermann,⊥ Ralf Bogumil,∥ and Herbert Witzel∥

Contribution from the Institute of Chemical Kinetics and Combustion, Novosibirsk 630090, Russia, Macromolecular Structure & Dynamics, Environmental Molecular Sciences Laboratory, Pacific Northwest Laboratory, Richland, Washington 99352, Fachrichtung Biophysik und Physikalische Grundlagen der Medizin, Universität des Saarlandes, 66421 Homburg (Saar), Germany, and Institute für Biochemie, Universität Münster, Münster, Germany

Received December 5, 1994[⊗]

Abstract: An orientationally-selected electron spin-echo envelope modulation (ESEEM) spectroscopy investigation was performed on VO^{2+} introduced into the high-affinity metal-binding site of D-xylose isomerase. The ESEEM spectra clearly reveal the presence of nitrogen ligands with hyperfine coupling $A^N \approx 6$ MHz. Detailed analysis includes first- and second-order treatment of the nitrogen basic and combination harmonics in two-pulse ESEEM spectra of the $g_\parallel$ and $g_\perp$ components. Complete determination of the hyperfine and quadrupole tensor indicates equatorial coordination of the imine nitrogen of the histidine residue. The presence of Cd^{2+} ion in the second, low-affinity metal-binding site does not affect the nitrogen couplings. The protons surrounding the VO^{2+} ion have been examined via the proton sum combinations in four-pulse ESEEM. They demonstrate the contribution of two protons probably belonging to the histidine ligand. These investigations strongly support the further application of VO^{2+} as a spin probe in conjunction with ESEEM spectroscopy for detailed investigation of nitrogen ligands in the active metal sites of proteins.

Introduction

The intracellular enzyme D-xylose isomerase from *Streptomyces ribiginosus* ATCC 21132 (XylI) catalyzes *in vivo* the reversible isomerization of α-D-xylose to α-D-xylulose.[1] The enzyme exists as a tetramer composed of four identical subunits with a M_r of 172 420.[2] The activity of the enzyme depends on divalent cations[1] which can occupy two binding sites in each subunit. The two binding sites have different affinities as determined by visible spectroscopy and activity measurements.[1-3] Recently, the two metal-binding sites of XylI were studied using VO^{2+} as a spectroscopic probe for visible, electron paramagnetic resonance (EPR), and electron nuclear double resonance (ENDOR) spectroscopies.[4] The VO^{2+} ion appears to inhibit enzymatic activity.[4] The data indicated that a nitrogen-containing ligand is involved in the ligand sphere of only the high-affinity metal-binding site denoted site B. The low-affinity site A was studied selectively by blocking site B with optically and EPR silent Cd^{2+}. The optical and EPR spectral characteristics of site A are consistent with a ligand environment composed of oxygen donors without nitrogen ligation. Coordination by nitrogen was also excluded by ENDOR measurements.[4]

Although ENDOR spectra of VO^{2+} in site B clearly show the presence of a nitrogen-containing ligand based on the existence of lines in the 4–9 MHz frequency region which are absent in site A spectra, unfortunately, they are not amenable to complete interpretation and quantitative determination of nitrogen hyperfine and quadrupole interactions due to the missing parts of the ENDOR spectra frequency region below than 3–4 MHz. This is connected with experimental problems in the ENDOR method. The nitrogen hyperfine coupling, 13.2 MHz, estimated from the ENDOR spectra is approximately twice the normal values reported for direct vanadyl–nitrogen coordination. In the present paper we report on the further investigation of the nitrogen ligand in site B of VO^{2+}-substituted XylI using electron spin-echo envelope modulation (ESEEM) spectroscopy.[5] This technique has been successfully applied to the study of nitrogens with weak hyperfine and quadrupole interactions in a large number of orientationally-disordered systems. It allows determination of nitrogen nuclear transitions to start from frequencies limited only by the decay times of the

* Address correspondence to Dr. S. A. Dikanov, MS&D, P7-55, Pacific Northwest Laboratory, P.O. Box 999, Richland, WA 99352.
† Institute of Chemical Kinetics and Combustion.
‡ Pacific Northwest Laboratory.
§ Alexander von Humboldt Foundation Research Fellow at Saarland University (06/01/92 to 10/31/93).
⊥ Universität des Saarlandes.
∥ Universität Münster.
⊗ Abstract published in *Advance ACS Abstracts,* April 15, 1995.

(1) (a) Chen, W. P. *Process Biochem.* **1980**, *15*, 30. (b) Chen, W. P. *Process Biochem.* **1980**, *15*, 36. (c) Verhoff, F. H.; Bogulawski, G.; Lantero, O. J.; Schloger, T. S.; Jao, Y. C. In *Comprehencive Biotechnology*; Balanch, H. W., Drew, S., Wang, D. I. C., Eds.; Pergamon Press: Oxford, 1985; Vol. 3, p 837.

(2) (a) Sudfeldt, C.; Schäffer, A.; Kägi, J.; Bogumil, R.; Schulz, H.-P.; Wulf, S.; Witzel, H. *Eur. J. Biochem.* **1990**, *193*, 863. (b) Karas, M.; Ingendoch, A.; Bahr, U.; Hillenkamp, F. *Biomed. Environ. Mass Spectrom.* **1989**, *18*, 841.

(3) (a) Sanchez, S.; Smiley, K. L. *Appl. Microbiol.* **1975**, *29*, 745. (b) Callens, M.; Tomme, P.; Kersters-Hilderson, H.; Cornelis, R.; Vangrysperre, W.; de Bruyne, C. K. *Biochem. J.* **1988**, *250*, 285. (c) Dauter, Z.; Dauter, M.; Hemker, J.; Witzel, H.; Wilson, K. S. *FEBS Lett.* **1989**, *247*, 1.

(4) Bogumil, R.; Hüttermann, J.; Kappl, R.; Stabler, R.; Sudfeldt, C.; Witzel, H. *Eur. J. Biochem.* **1991**, *196*, 305.

(5) (a) *Advanced EPR. Applications in Biology and Biochemistry*; Hoff, A. J., Ed.; Elsevier: Amsterdam, 1989. (b) *Modern Pulsed and Continuous-Wave Electron Spin Resonance*; Kevan, L., Bowman, M. K., Eds., Wiley: New York, 1990. (c) Dikanov, S. A.; Tsvetkov, Yu. D. *Electron Spin Echo Envelope Modulation (ESEEM) Spectroscopy*; CRC Press: Boca Raton, FL, 1992.

0002-7863/95/1517-4976$09.00/0

echo envelopes, $1/T_2$ or $1/T_1$, i.e., in practice from values of a few hundredths or tenths of a megahertz.

The characterization of VO^{2+} with nitrogen-containing ligands by orientationally-selected, two-dimensional, and multifrequency ESEEM spectroscopy has been the subject of interest for several years.[6-9] Nitrogen coordination to vanadyl centers has been discovered and investigated by ESEEM spectroscopy in the following proteins: bromoperoxidase,[10] lactoferrin and transferrin,[11] pyruvate kinase,[12] apoferritin,[13] and *S*-adenosylmethionine synthetase.[14] Through the measurements of hyperfine and quadrupole nitrogen constants, the type of ligand and the coordination geometry have been established. In this work, the nitrogen ESEEM is studied using two- and three-pulse electron spin-echo (ESE) sequences in conjunction with orientation selection via the excitation of special points in the powder EPR spectra corresponding to the principal directions of **g** and **A**(^{51}V) tensors. In addition, the observation of sum combinations in the one-dimensional four-pulse ESE sequence[15] is used to detect protons located in the nearest surroundings of the VO^{2+} ion.

Experimental Methods

Samples. The materials used and the sample preparation were as described previously.[4] Two samples were studied. One is XylI titrated with 4 equiv of VO^{2+} per tetramer (denoted $4VO^{2+}$); the other was obtained after treatment with four VO^{2+} ions and, subsequently, with four Cd^{2+} ions. This sample is denoted below as $4VO^{2+}/4Cd^{2+}$.

ESE Equipment. X-band pulsed EPR experiments (~9.8 GHz) were performed using a Bruker ESP 380 spectrometer with a dielectric low *Q* cavity. The length of a $\pi/2$ pulse was 16 ns. Four-step phase cycles $+(0,0,0)$, $-(0,\pi,0)$, $-(\pi,0,0)$, $+(\pi,\pi,0)$ in the three $\pi/2$ pulse sequence[16] and $+(0,0,0,0)$, $-(0,0,0,\pi)$, $+(0,0,\pi,0)$, $-(0,0,\pi,\pi)$ in the four-pulse sequence[17] were used to eliminate unwanted features from echo envelopes. In a one-dimensional version of the four-pulse HYSCORE experiment $\pi/2-\tau-\pi/2-t_1-\pi-t_2-\pi/2-\tau-$echo,[18] the refocusing π pulse was applied such that $t_1 = t_2 = T/2$ and the echo amplitude was recorded as a function of the time T which was increased in a stepwise manner.[17,19] The experiments were performed at 4–8 K using an Oxford CF 935 cryostat. Cosine and modulus Fourier-transformed (FT) ESEEM spectra were obtained without restoration of the dead time region after normalizing the modulating by the relaxation decay and subtracting the average value. Dead times were 120 ns for two-pulse envelopes and τ + 24 ns for three- and four-pulse ESEEM. Simulations took these dead times into account.

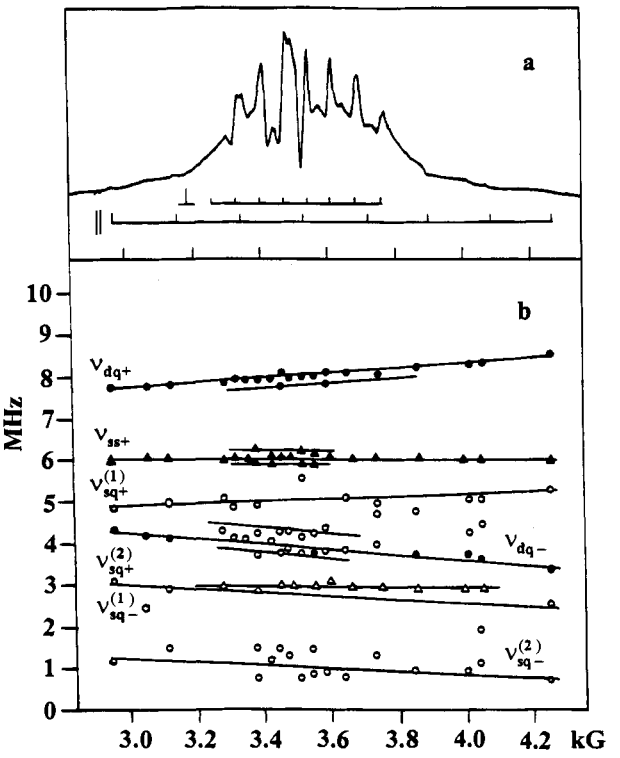

Figure 1. Two-pulse field sweep ESE spectrum of the $4VO^{2+}/4Cd^{2+}$ sample (0.27 mM XylI in 0.05 M maleic acid, pH 6.7) at the microwave frequency 9.806 GHz (a) and the frequencies of the well-resolved lines in the two-pulse ESEEM spectra of the $4VO^{2+}/4Cd^{2+}$ sample at different magnetic fields (b).

Results

Nitrogen ESEEM. The two-pulse ESE-detected EPR spectra of $4VO^{2+}/4Cd^{2+}$ and $4VO^{2+}$ samples are shown in Figures 1a and 2a. These spectra are typical for orientationally-disordered VO^{2+} complexes in frozen solutions with well-pronounced $g_{\|}$ and $g_{\perp}$ features for the eight ^{51}V powder hyperfine components. At the same time the EPR lineforms of these samples clearly show differences in agreement with previous observations by continuous wave (CW) EPR spectra.[4] In both these samples the VO^{2+} ions occupy the binding site B with high affinity. However, the second binding sites A are free in the first sample and, conversely, are occupied by Cd^{2+} ions in the second sample. The metal-binding sites are only 4.9 Å apart,[20] and one residue (Glu216) should ligate both sites. Therefore, it seems resonable to assume that ion binding to site A can influence the geometry of the ligand environment in site B, leading to the different **g** and **A** tensors of VO^{2+} already described.[4]

Figure 3 depicts typical two- and four-pulse ESE envelopes of $4VO^{2+}/4Cd^{2+}$ obtained on the $g_{\|}(m_I=+7/2)$ component at a magnetic field of 2960 G. Corresponding ESEEM spectra contain lines in the region 0–12 MHz and also peaks around the basic and the double proton Zeeman frequencies. As in ENDOR spectra, the lines in the former region are related to nitrogen nuclear transitions. Selected two-pulse cosine FT ESEEM spectra covering only the frequency region 0–14 MHz are given in Figure 4. They exhibit lines with positive and with negative amplitudes. According to Mims's theoretical results[21]

(6) Astashkin, A. V.; Dikanov, S. A.; Tsvetkov, Yu. D. *Zh. Struct. Khim.* **1985**, *26* (3), 53; *J. Struct. Chem.* **1985**, *26*, 363.
(7) (a) Reijerse, E. J.; Shane, J.; de Boer, E.; Collison, D. In *Electron Magnetic Resonance of Disordered Systems*; Yordanov, N. D., Ed.; World Scientific: Singapore, 1989; p 189. (b) Reijerse, E. J.; Shane, J.; de Boer, E.; Höfer, P.; Collison, D. In *Electron Magnetic Resonance of Disordered Systems*; Yordanov, N. D., Ed.; World Scientific: Singapore, 1991; p 253.
(8) Cosgrove-Larsen, S. A.; Singel, D. J. *J. Phys. Chem.* **1992**, *96*, 9007.
(9) Togni, A.; Rist, G.; Rihs, G.; Schweiger, A. *J. Am. Chem. Soc.* **1993**, *115*, 1908.
(10) De Boer, E.; Keijzers, C. P.; Klaassen, A. A. K.; Reijerse, E. J.; Collison, D.; Garner, C. D.; Wever, R. *FEBS Lett.* **1988**, *235*, 93.
(11) Eaton, S. S.; Dubach, J.; More, K. M.; Eaton, G. R.; Thurman, G.; Ambruso, D. R. *J. Biol. Chem.* **1989**, *264*, 4776.
(12) Tipton, P. A.; McCracken, J.; Cornelius, J. B.; Peisach, J. *Biochemistry* **1989**, *28*, 5720.
(13) Gerfen, G. J.; Hanna, P. M.; Chasteen, N. D.; Singel, D. J. *J. Am. Chem. Soc.* **1991**, *113*, 9513.
(14) Zhang, C.; Markham, G. D.; LoBrutto, R. *Biochemistry* **1993**, *32*, 9866.
(15) Tyryshkin, A. M., Dikanov, S. A.; Goldfarb, D. *J. Magn. Reson., Ser. A* **1993**, *105*, 271.
(16) Fauth, J.-M.; Schweiger, A.; Braunschweiler, L.; Forrer, J.; Ernst, R. R. *J. Magn. Reson.* **1986**, *66*, 74.
(17) Gemperle, C.; Aebli, G.; Schweiger, A.; Ernst, R. R. *J. Magn. Reson.* **1990**, *88*, 241.
(18) Höfer, P.; Grupp, A.; Nebenführ, H.; Mehring, M. *Chem. Phys. Lett.* **1986**, *132*, 279.
(19) Schweiger, A. In *Modern Pulsed and Continuous-Wave Electron Spin Resonance*; Kevan, L., Bowman, M. K., Eds.; Wiley: New York, 1990; p 43.
(20) Collyer, C. A.; Henrick, K.; Blow, D. M. *J. Mol. Biol.* **1990**, *212*, 211.
(21) Mims, W. B. *Phys. Rev. B* **1972**, *6*, 3543.

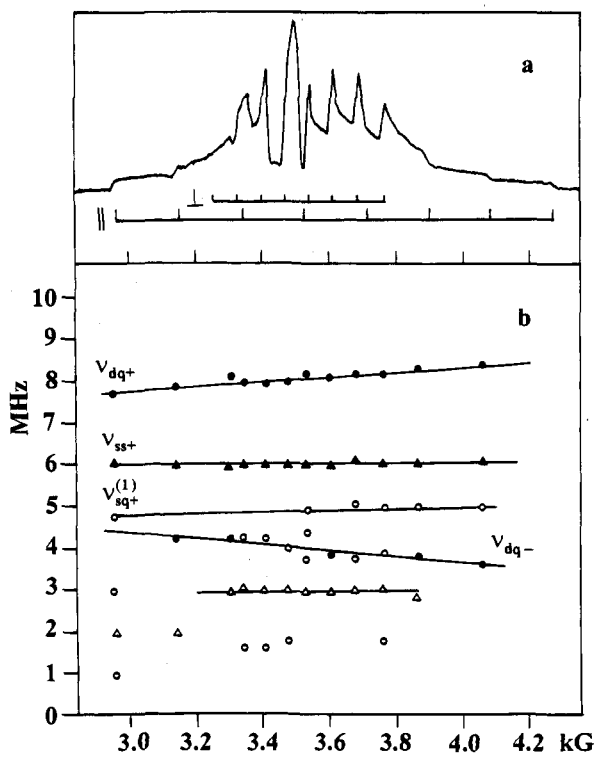

Figure 2. Same as Figure 1 for the $4VO^{2+}$ sample.

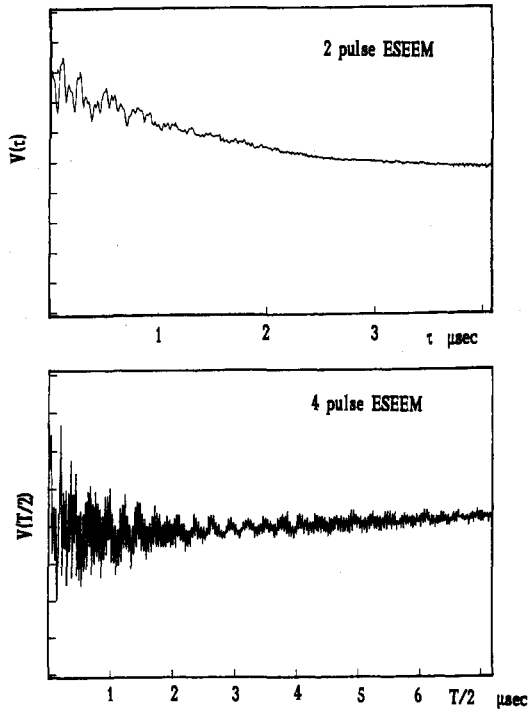

Figure 3. Two- and four-pulse ESE envelopes of the $4VO^{2+}/4Cd^{2+}$ enzyme obtained on the $g_{||}$ component of the EPR spectrum at the magnetic field 2960 G.

the primary ESEEM contains frequencies of the basic nuclear transitions from each of the two $m_S = \pm 1/2$ electron spin manifolds, which for $I = 1$ includes two single-quantum, $\nu^{(1)}_{sq\pm}$ and $\nu^{(2)}_{sq\pm}$, transitions and one double-quantum, $\nu_{dq\pm}$, transition. The primary ESEEM spectra also contain combination harmonics with one frequency from the positive and one from the negative electron spin manifold. There are three types of possible combinations, $\nu^{(i)}_{sq+} \pm \nu^{(j)}_{sq-}$, $\nu_{dq\pm} \pm \nu^{(i)}_{sq\pm}$, $\nu_{dq+} \pm \nu_{dq-}$ $(i, j = 1,2)$, which differ in frequency (see the Appendix).

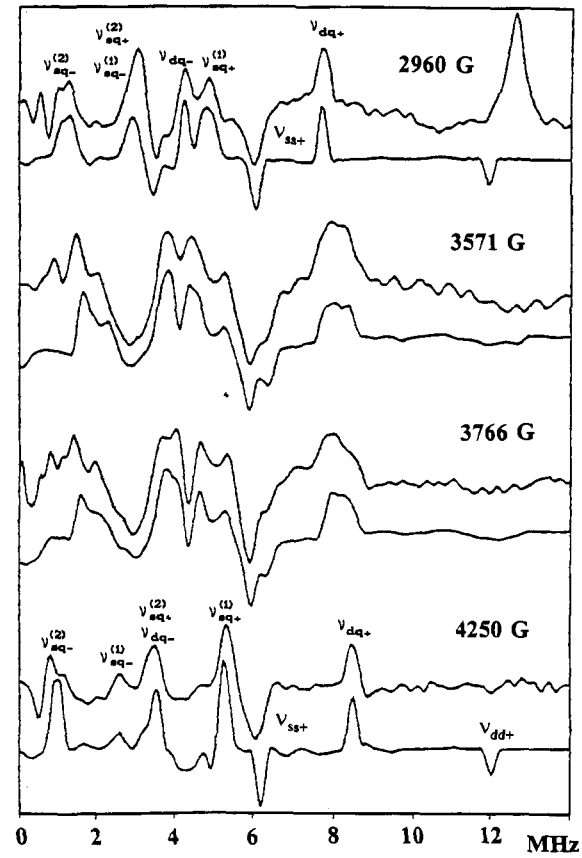

Figure 4. Nitrogen cosine two-pulse FT ESEEM spectra of the $4VO^{2+}/4Cd^{2+}$ enzyme obtained at different points of the EPR spectrum (top) and corresponding simulated spectra (bottom) with the same parameters as Figure 5A (see the caption of Figure 5).

Figures 1b and 2b also depict the modulation frequencies manifested in primary ESEEM spectra at different values of the external magnetic field at the $g_{||}$ and $g_{\perp}$ components.

"Single-Crystal-Like" Spectra at $g_{||}$. It is convenient to start the quantitative analysis of the experimental data from spectra for the $4VO^{2+}/4Cd^{2+}$ enzyme obtained at $g_{||}(m_I=+7/2)$ and $g_{||}$-$(m_I=-7/2)$ at the extreme ends of the EPR spectra at magnetic fields 2960 and 4250 G. Under microwave excitation at these spectral positions, the echo signals are formed by complexes with their axis approximately parallel to the external magnetic field, and therefore the ESEEM can be considered as single-crystal-like. The spectra recorded at low field, 2960 G (corresponding to a ^{14}N Zeeman frequency $\nu_I = 0.91$ MHz), contain five well-pronounced components with positive amplitude at the frequencies 7.76, 4.88, 4.30, 3.08, and 1.2 MHz (the accuracy in the determination of line maxima is 0.03 MHz) (Figure 4, top). These can be interpreted as a superposition of two triplets, 7.76, 4.88, and 3.08 MHz and 4.30, 3.08, and 1.2 MHz, of the six nitrogen nuclear transitions from both m_S manifolds. With increasing magnetic field, the frequencies of the first triplet should also increase and those of the second one decrease. The frequencies of the single-quantum transitions change with $|\Delta\nu_I|$ and those of the double-quantum transitions with $2|\Delta\nu_I|$. Therefore, at the high field of 4250 G ($\nu_I = 1.31$ MHz) the two triplets are expected at the frequencies 8.56, 5.28, and 3.5 MHz and 3.5, 2.68, and 0.8 MHz which correspond well to the five experimentally observed lines at 8.56, 5.38, 3.48, 2.64, and 0.88 MHz (Figure 4, bottom).

First-order expressions for all ^{14}N frequencies that can appear in two-pulse ESEEM are given in the Appendix (eq A1). Using them, one can find nitrogen hyperfine $A^N_{||} = 6.15 \pm 0.05$ MHz

Table 1. Coefficients (MHz^{-1}) Describing the Field Dependence of the Second-Order Contribution to ESEEM Harmonics and Their Numerical Comparison at $A_{||} = 6$ MHz

ESEEM harmonic	coefficient	$\nu_I = 0.91$ MHz	$\nu_I = 1.31$ MHz
$\nu_{sq+}^{(1,2)}$	$1/2(A_{||}/2 + \nu_I)$	0.13	0.12
$\nu_{sq-}^{(1,2)}$	$1/2(A_{||}/2 - \nu_I)$	0.24	0.30
ν_{dq+}	$1/(A_{||}/2 + \nu_I)$	0.255	0.23
ν_{dq-}	$1/(A_{||}/2 - \nu_I)$	0.48	0.59
ν_{ss+}	$A_{||}/2(A_{||}^2/4 - \nu_I^2)$	0.37	0.41
ν_{dd-}	$2\nu_I/(A_{||}^2/4 - \nu_I^2)$	0.22	0.36

and quadrupole $Q_{||}^N = 0.61 \pm 0.02$ MHz coupling from the four pairs of single-quantum peaks $\nu_{sq\pm}^{(1)}$ and $\nu_{sq\pm}^{(2)}$ in two $g_{||}$ spectra. Employing the position of the ν_{dq+} and ν_{dq-} lines, one determines $A_{||}^N$ of 5.94 and 6.11 MHz, respectively, from the spectra at low and high fields.

The spectra obtained at the $g_{||}$ components also exhibit a line with negative amplitude at 6.00−6.05 MHz, which can be attributed reasonably to the sum combination of single-quantum transitions. Only the combinations $\nu_{sq+}^{(1)} + \nu_{sq-}^{(2)}$ and $\nu_{sq+}^{(2)} + \nu_{sq-}^{(1)}$ (which sum to $A_{||}^N$ in first order) contribute to this line (to be denoted as ν_{ss+}). Two other harmonics of this type are shifted by $\pm 3Q_{||}^N$ and thus should give lines at about 4.4 and 8.0 MHz, where they would overlap with the more intense basic frequencies. Among the other spectral features in the $g_{||}$ spectra, note the weak line with negative amplitude at a frequency (~12.0−12.1 MHz) close to twice the hyperfine constant of nitrogen. It is connected with the sum of double-quantum transitions ν_{dd+}.

Second-Order Contribution to ESEEM Harmonics. The nitrogen hyperfine couplings estimated using the first-order treatment exibit small discrepancies. The discrepancy of ~0.2 MHz between $A_{||}^N$ from the ν_{dq+} peak position and the sum of maxima of the $\nu_{sq+}^{(1)}$ and $\nu_{sq+}^{(2)}$ lines probably arises from the overlap of at least one single-quantum transition with another line in each $g_{||}$ spectrum ($\nu_{sq+}^{(2)}$ with $\nu_{sq-}^{(1)}$ in the low-field spectrum, $\nu_{sq+}^{(2)}$ with ν_{dq-} in the high-field one). However, the maxima of the ν_{dq+}, ν_{ss+}, and ν_{dq-} lines in the low-field $g_{||}$ spectrum are clearly visible. Therefore, any discrepancies in hyperfine couplings obtained from these harmonics are attributed to second-order contributions which vary for the different modulation harmonics (see eq A2). The second-order contribution to the hyperfine coupling depends on the order of the harmonic and the magnetic field. Table 1 collects the coefficients determining the field dependence of the second-order terms and their numerical values at $\nu_I = 0.91$ and 1.31 MHz for $A_{||}^N = 6$ MHz. These estimates of the second-order contribution indicate that its value for ν_{dq+} is approximately 2 times smaller than for ν_{dq-} and 1.5 times smaller than for ν_{ss+}. Those ratios correspond well to differences found for hyperfine couplings and allow correction of the nitrogen hyperfine constant to $A_{||}^N \simeq 5.7$ MHz.

The corrected value for the hyperfine coupling $A_{||}^N$ and the second-order term $A_{||}^{(2)}$ can be calculated directly from the position of the two double-quantum transitions $\nu_{dq\pm}$ in the $g_{||}$ spectra by the following equations

$$A_{||}^N = 2\nu_I(\nu_{dq+} + \nu_{dq-})/[8\nu_I - (\nu_{dq+} - \nu_{dq-})] \quad (1)$$

$$A_{||}^{(2)} = 1/2[\nu_{dq\pm} - (A_{||}^N \pm 2\nu_I)](A_{||}^N \pm 2\nu_I)$$

derived from expressions A2 for $\nu_{dq\pm}$. Both these double-quantum lines at 7.76 and 4.3 MHz are clearly resolved in the low-field $g_{||}$ spectrum. They give $A_{||}^N = 5.74 \pm 0.04$ MHz and $A_{||}^{(2)} = 0.75 \pm 0.12$ MHz^2.

The above analysis does not provide strong evidence for a measurable second-order contribution to the nitrogen quadrupole coupling exceeding the accuracy of the line positions and can be estimated at a few hundredths of a megahertz. Therefore, using $Q_{||}^N = 0.61$ MHz from the first-order treatment and neglecting the contribution of $B^2/4$ (numerical simulations discussed later confirm its value to be a few hundredths of a square megahertz), one can estimate $K^2(3 + \eta^2) = 1.03 \pm 0.12$ MHz^2. This limits the possible values to $0.5 < K < 0.58$ MHz (±0.03 MHz).

Independent evidence of the second-order contribution follows from the deviation of the $\nu_{dd-} = \nu_{dq+} - \nu_{dq-}$ harmonic from $4\nu_I$. The ν_{dd-} harmonic in $g_{||}$ low-field spectra has a negative amplitude with a maximum at ~3.5 MHz. However, its position can be distorted by overlap with the more intense line of the basic transition with positive amplitude. Instead of a direct measurement, ν_{dd-} can be calculated from the difference in the ν_{dq+} and ν_{dq-} peak positions. Their difference of 3.46 MHz is smaller than $4\nu_I$ by 0.18 MHz. The absolute value of the second-order contributions to ν_{ss+}, and ν_{dd-} scale as $A_{||}^N/4\nu_I$. This gives ~0.3 MHz for ν_{ss+} when $A_{||}^N \simeq 6$ MHz. This leads again to a second-order corrected hyperfine constant of 5.70−5.75 MHz.

Field and Orientation Dependence of Nitrogen ESEEM Spectra. In Figures 1b and 2b the frequency positions of the most pronounced and well-resolved features of two-pulse ESEEM spectra are plotted against the magnetic field. The points presented show that ν_{dq+} and ν_{ss+} are clearly visible at all field values for both enzymes. The frequency of ν_{dq+} increases approximately linearly with the magnetic field. This relationship is fulfilled clearly for ESEEM lines on the left and right sides of the EPR spectra at the $g_{||}$ components ($g_{||}$ region). In the middle section ($g_\perp$ region), there is a scatter in the ν_{dq+} frequencies around a straight line. The same effect holds for ν_{ss+} whose position 6.00−6.05 MHz is nearly independent of the field in the $g_{||}$ region and deviates from this value in the $g_\perp$ region. Figure 4 provides visual confirmation of such behavior for the ν_{dq+} and ν_{ss+} peaks. The line shape of ν_{dq+} in spectra from the $g_\perp$ region is broader and more asymmetric than in spectra from the $g_{||}$ region. The ν_{ss+} line also has an asymmetric form, and its maximum is shifted to frequencies lower than ~6.0 MHz in the $g_\perp$ spectra. In some spectra, these peaks have slight splittings indicated in Figure 1b by two points at the same field for one transition. The two shoulders on the ν_{ss+} line can be used for direct estimation of the nitrogen hyperfine couplings in the plane perpendicular to the V=O bond. As seen from Figure 1b all other transitions for the $4VO^{2+}/4Cd^{2+}$ enzyme can be correlated more or less satisfactorily with a linear dependence on the magnetic field in the $g_{||}$ region. The increased spread of peak positions in the $g_\perp$ region makes the study of their behavior difficult.

Figures 1b and 2b demonstrate a similar frequency versus field dependence of ν_{dq+}, ν_{ss+}, $\nu_{sq+}^{(1)}$, and ν_{dq-} lines for both enzymes. This similarity indicates identical coupling for the unpaired electron spin with the ligand nitrogen. However, due to shorter relaxation decay times for the two-pulse envelopes in the $4VO^{2+}$ samples, the spectral features at the lower frequencies (≤2 MHz) were not resolved as well as in the spectra of the $4VO^{2+}/4Cd^{2+}$ sample. The spectra of both enzymes exibit a broad line with negative amplitude at a frequency of ~3 MHz only in the $g_\perp$ region which can be

attributed to the difference combination $\nu_{dq\pm} - \nu_{sq\mp}$. This line masks the field variations of $\nu^{(2)}_{sq+}$ and $\nu^{(1)}_{sq-}$ frequencies in the $g_\perp$ region.

Additional information about the nitrogen hyperfine and quadrupole constants can be obtained using the special variation of $\nu_{dq\pm}{}^2/4 - \nu_I{}^2$ as a function of $\pm\nu_I$ for the higher and lower double-quantum transitions, respectively.[22] The variation for the $\nu_{dq\pm}$ peaks of both enzymes (depicted in Figures 1b and 2b by black circles) shows a linear behavior with a slope of 6.0 ± 0.1 MHz. At the same time we were unable to get any information from the intercept value, probably due to a contribution from nonsecular hyperfine terms[22] which were not taken into account in this approach.

Simulations of ESEEM Spectra. Simulations of ESEEM spectra were first applied to the $g_{||}$ points. Using the interpretation given above, it was possible to obtain good agreement between experimental and simulated spectra with $A^N_{||} = 5.7$ MHz and $Q^N_{||} = 0.64$ MHz at low and high fields. These simulations place some limitations on the principal values of the nitrogen anisotropic hyperfine interaction (hfi) T_{11} (or $T_\perp$) < 0.6 MHz and nuclear quadrupole interaction (nqi) $0.45 \le K \le 0.6$ MHz (in a good correspondence with estimates from the second-order contribution), $\eta = 0.5-1.0$, and their relative orientation in the coordinate system of the vanadium hyperfine tensor. In part these limitations follow from the explicit expressions A3 and A4 deriving $A^N_{||} = 5.7$ MHz and $Q^N_{||} = 0.64$ MHz from the principal elements of the corresponding tensors. During the simulations additional constraints appeared from the correlated variations of different parameters in eqs A3 and A4. For example, the patterns with $\eta < 0.5$ usually show the ν_{dd-} harmonic at lower frequencies than the experimentally observed line at 3.5 MHz in the spectrum at 2960 G. Therefore, it overlaps with the more intense lines from the single-quantum transitions. Furthermore, the simulations with K values not satisfying the inequality $0.45 \le K \le 0.6$ MHz reproduce the positions of all lines in experimental spectra, however, with significantly different relative intensities. The conclusion T_{11} ($T_\perp$) < 0.6 MHz is based on the observation that the variations of T_{11} ($T_\perp$) in that range do not lead to significant changes of simulated $g_{||}$ spectra.

Complete analysis of ESEEM spectra recorded at other points of the EPR spectrum including $g_\perp$ positions requires much more effort because they correspond to the case of a partially-oriented system with anisotropic spectral lines. For a more detailed understanding of the origin of the lines presented in the experimental $g_\perp$ spectra, a series of simulations with quadrupole parameters satisfying the above limitations and relation A4 were performed. The main emphasis was placed on the anisotropic lineform and the positions of the maxima of all basic ν_{sq} and ν_{dq} harmonics and their combinations $\nu_{ss\pm}$ and $\nu_{dd\pm}$. At the same time no evidence was found of a noticeable contribution to the $g_\perp$ spectra of lines representing the combinations $\nu^{(i)}_{sq+} + \nu^{(i)}_{sq-}$, $\nu^{(i)}_{sq+} - \nu^{(j)}_{sq-}$, and $\nu_{dq\pm} \pm \nu^{(i)}_{sq\pm}$ ($i, j = 1, 2$, $i \neq j$), in agreement with theoretical considerations[23] for the case $A > 2\nu_I$.

From these simulations, it was possible to interpret the experimental $g_\perp$ spectrum at the field 3571 G as shown in Figure 5C. This interpretation confirms the noticeably anisotropic lineform of almost all recognized lines (especially ν_{sq}) producing two or even more maxima. The different components strongly overlap in the frequency region 3−5.5 MHz, additionally complicating the $g_\perp$ spectra. It seems, however, that reaching even the present level of understanding of $g_\perp$ spectra could be very problematic without data from the $g_{||}$ spectra and the model simulations.

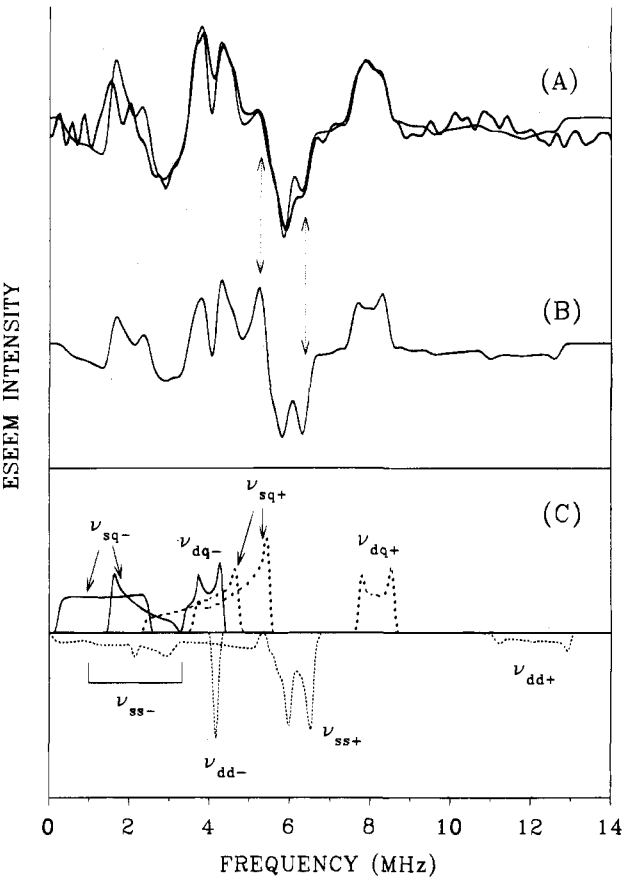

Figure 5. Illustration of the different stages in the simulation of the $g_\perp$ spectrum at 3571 G (see text for details). Parameters used for the simulation of spectra A and B: hfi tensor, $a = 5.65 \pm 0.05$ MHz, $T_{11} = 0.4$ MHz ± 0.05 MHz, $T_{22}/T_{11} = 0.1 \pm 0.1$; Euler angles of the principal axes of the hfi tensor in the frame of the ^{51}V hfi tensor, $\phi = 20°$, $\theta = 80°$, $\psi = -55°$; nqi tensor, $K = 0.5 \pm 0.03$ MHz, $\eta \simeq 1$; Euler angles of the principal axes of the nqi tensor, $\alpha = -35°$, $\beta = 90°$, $\gamma = -20° \pm \sim 5°$; **g** tensor, $g_x = g_y = 1.977$, $g_z = 1.939$; ^{51}V hfi tensor, $A_z = 182$ G, $A_x = A_y = 63$ G (for spectrum B) and $A_x = 62$ G, $A_y = 64$ G (for spectrum A and the spectra in Figure 4).

The interpretation given yields additional limitations on the coupling parameters with nitrogen from the positions of some lines in the $g_\perp$ spectra. For instance, ν_{ss+} manifests itself as an asymmetric doublet with negative amplitude and minima at the frequencies 5.9 and 6.3 MHz. The doublet (instead of the singlet in $g_{||}$ spectra) is formed due to the anisotropy of the nitrogen hfi in the equatorial plane. The line positions correspond in first order to the diagonal elements $A^N_{\perp(1)}$ and $A^N_{\perp(2)}$ of the tensor. It is better to use the second-order corrected formula to evaluate $A^N_{\perp(1,2)}$. The simulation of ESEEM spectra at the $g_{||}$ components confirms the second-order corrected $A^N_{||} = 5.7$ MHz. The positions of the ν_{ss+} line in $g_{||}$ and $g_\perp$ spectra indicate that the second-order contribution of ~0.3−0.4 MHz to the hyperfine coupling is comparable to the anisotropy of the nitrogen hfi. Assuming slight variations in the second-order contribution to ν_{ss+} at different orientations of the magnetic field and taking its value as ≃0.35−0.4 MHz from the analysis of $g_{||}$ spectra, one can estimate $A^N_{\perp(1)} = 5.5$ MHz and $A^N_{\perp(2)} = 5.9$ MHz. Thus, the isotropic hfi constant is $a = 1/3(A^N_{||} + A^N_{\perp(1)} + A^N_{\perp(2)}) = 5.7$ MHz, and the diagonal elements of the anisotropic

(22) (a) Cosgrove, S. A.; Singel, D. J. *J. Phys. Chem.* **1990**, *94*, 8393. (b) Cosgrove, S. A.; Singel, D. J. *J. Phys. Chem.* **1990**, *94*, 2619.
(23) Flanagan, H. L.; Singel, D. J. *J. Chem. Phys.* **1988**, *89*, 2585.

hfi tensor in the coordinate system specified by the vanadium hfi are $T_{||} \simeq 0$ and $T_{\perp(1)} = -T_{\perp(2)} = -0.2$ MHz.

According to model simulations, the $\nu^{(2)}_{sq+}$ transition in $g_\perp$ spectra possesses an extended line shape limited by maxima at the frequencies 3.5 and 5.2 MHz. The additional maximum at ~4.5 MHz is created by the overlap of the $\nu^{(1)}_{sq+}$, ν_{dq-}, and ν_{dd-} lines. The analytical expression for the $\nu^{(2)}_{sq+}$ frequency at different orientations of the magnetic field in the perpendicular plane is given even in first order by a rather complex formula (see eqs A5 and A6). Therefore, the direct method using line maxima was impossible in this case. However, some definite characteristics in the $\nu^{(2)}_{sq+}$ lineform were discovered during simulations with different angles ψ and γ for the hfi and nqi tensor orientation in the perpendicular plane. For coaxial tensor axes in this plane the maxima of $\nu^{(2)}_{sq+}$ at 3.5 and 5.2 MHz appear as very narrow and intense lines, and obviously do not correspond to the experimental line shapes. The increase in line width and the decrease in their intensities nearing the experimental ones take place at $\psi \simeq [\gamma + (45° \pm 10°) + 90°n]$, $n = 0, 1, 2, ...$

The estimated small anisotropy in the hfi suggests that the observed $\nu^{(2)}_{sq+}$ line shape is mainly determined by the anisotropy of the nitrogen nqi tensor. For a relative shift of nqi and hfi tensor axes in the plane by an angle of ~45°, one can find the diagonal elements of the nqi tensor $Q^N_{\perp(1)}$ and $Q^N_{\perp(2)}$ in first order from the maximum positions 3.5 and 5.2 MHz assuming $A^N_\perp(\chi = 45°) \simeq (A^N_{\perp(1)} + A^N_{\perp(2)})/2 \simeq a$. This procedure gives $Q^N_{\perp(1)} = 0.17$ MHz and $Q^N_{\perp(2)} = -0.83$ MHz. This estimate is confirmed by the sum (which is close to zero) of these elements with $Q^N_{||} = 0.64$ MHz determined in the independent analysis of the $g_{||}$ spectra.

Summarizing the considerations above, let us note once more the following ordered set of limitations on the nitrogen coupling parameters: (a) $0.45 \le K \le 0.6$ MHz, $\eta < 0.5$; (b) $A^N_{||} = 5.7$ MHz, $A^N_{\perp(1)} = 5.5$ MHz, $A^N_{\perp(2)} = 5.9$ MHz, $a = 5.7$ MHz; (c) $Q^N_{||} = 0.64$ MHz, $Q^N_{\perp(1)} = 0.17$ MHz, $Q^N_{\perp(2)} = -0.83$ MHz; (d) $|\psi - \gamma| \simeq (45° \pm 10°) + 90°n$, which is the angle between the $A^N_{\perp(1)}$ and $Q^N_{\perp(1)}$ directions. A^N_i and Q^N_i are derived by eqs A3 and A4. Although it is impossible to solve this system of equations, together with additional existing limitations, they form a good basis for final optimum simulations of ESEEM spectra at the $g_{||}$ and $g_\perp$ components. However, it has been discovered during such simulations that the intensity and width of the peaks at 3.5 and 5.2 MHz for the $\nu^{(2)}_{sq+}$ line and the two components of the ν_{ss+} doublet always remain nearly equal at all possible nitrogen couplings as in Figure 5B. One can rationalize the necessary asymmetry in line intensities by the introduction of additional orientational selection in the xy equatorial plane, for example, via the hfi rhombicity of the vanadium nucleus. This effect appears already when the difference between the vanadium hfi tensor components in this plane of only a few gauss reaches the pulse excitation width on the order of the microwave pulse strength $H_1 = 3-5$ G. It is clearly demonstrated by the spectrum in Figure 5A calculated with $\Delta A_{xy} = A^v_y - A^v_x = 2$ G and $H_1 = 3$ G which shows better correspondence with the experimental spectrum (noisy trace of Figure 5A) in both line positions and intensities.

According to the data of Bogumil et al.,[4] the $A^v_\perp$ component of the vanadium hfi tensor demonstrates the most significant variation in the presence of a nitrogen-containing ligand compared to other characteristics of ESR spectra. In principle, one can expect that the introduction of a single nitrogen ligand may create vanadium hfi rhombicity when all other ligands are coordinated by oxygen. However, if the induced rhombicity is on the order of only a few gauss, it cannot be resolved in EPR spectra of a frozen solution. At the same time the echo envelopes formed by the microwave pulses with amplitudes of 3−5 G appear to be sensitive and to develop additional orientational selection with this level of rhombicity. The nitrogen coordination may accompany **g** tensor rhombicity as well, although we introduced the additional orientational selection in the xy plane via only the rhombicity of vanadium hfi. Note finally, that ESEEM simulations do not allow the determination of the actual value of vanadium hfi rhombicity but only its magnitude in relation to the excitation width H_1. The calculation with $\Delta A_{xy} = 3$ G and $H_1 = 5$ G gives an ESEEM spectrum similar to those depicted in Figure 5A.

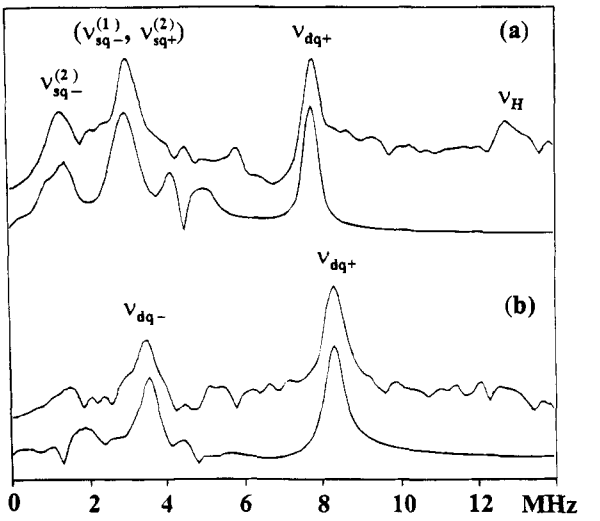

Figure 6. Experimental (top) and calculated (bottom) three-pulse modulus FT ESEEM spectra obtained at $\tau = 152$ ns in the fields 2960 G (a) and 4250 G (b).

The analysis performed and the parameters determined during the two-pulse ESEEM simulations are confirmed in three-pulse spectra. Those obtained at $\tau = 152$ ns at the $g_{||}$ components in low and high field contain the double-quantum transition ν_{dq+} at the frequencies 7.78 and 8.54 MHz, respectively. They shift by a value close to $2\Delta\nu_I = 0.8$ MHz corresponding to the magnetic field difference of the two points. The other double-quantum transition ν_{dq-} at 3.5 MHz is observed only in the spectra recorded at high field. In the low-field spectrum the ν_{dq-} line at the frequency ~4.3 MHz is not developed due to the well-known suppression effect.[21] Instead of this, line peaks at the single-quantum transitions $\nu^{(2)}_{sq-}$, $\nu^{(1)}_{sq-}$, and $\nu^{(2)}_{sq+}$ appear. Simulated three-pulse ESEEM spectra satisfactorily reproduce this behavior of the ν_{dq-} harmonic (Figure 6).

Proton ESEEM. Together with peaks in the region 0−12 MHz attributed to the nitrogen, two- and four-pulse ESEEM spectra contain lines in the region of single and double Zeeman proton frequencies from protons located in the surroundings of the metal-binding site. Our main interest in the proton spectra was connected with the investigation of additional sum combinations shifted relative to the matrix line at $2\nu_I$ produced by very remote protons. Recent investigations have shown that such shifted lines appear from protons located close to the paramagnetic ion, i.e., belonging to the ligand molecules. Their shifts are sensitive to the distance and orientation of the protons relative to the metal complex coordinate system.[13,15,24] The two-pulse ESE envelopes of VO^{2+} in XylI demonstrate a relatively fast decay limited by the electronic relaxation time T_2. The

(24) Tyryshkin, A. M.; Dikanov, S. A.; Evelo, R. G.; Hoff, A. J. *J. Chem. Phys.* **1992**, *97*, 42.

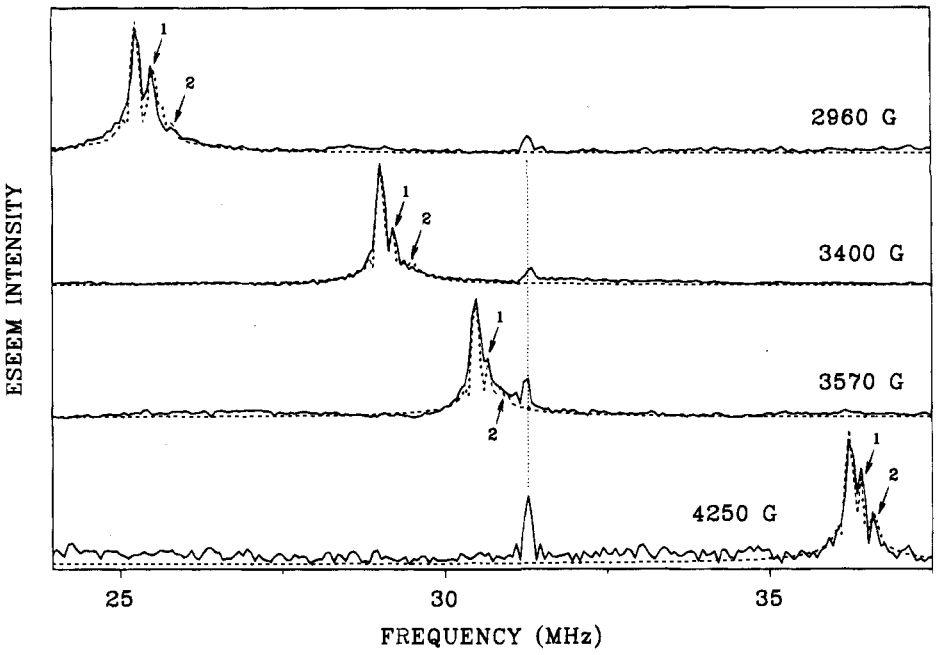

Figure 7. Experimental (solid line) and calculated (dashed line) four-pulse modulus FT ESEEM spectra of $4VO^{2+}/4Cd^{2+}$ in the region of proton double Zeeman frequencies. Time τ: 264 ns for the spectrum at 2960 G, 248 ns (3400 and 4250 G), and 232 ns (3570 G). The peaks on 31.2 MHz connected by the dotted line are an artifact of the spectrometer.

corresponding spectra clearly showed the existence of at least one line shifted to higher frequencies from the proton $2\nu_I$, but gave, however, no complete resolution in this region. The use of a one-dimensional four-pulse sequence has allowed improved resolution.

Theoretical expression of one-dimensional four-pulse ESEEM for the $S = 1/2$, $I = 1/2$ system contains the same set of frequencies as two-pulse ESEEM, i.e., two basic nuclear frequencies and their sum and difference combinations.[15,17] The distinction is only that amplitude coefficients of modulation frequencies in four-pulse ESEEM contain additional terms depending on the time τ between first and second pulses which is kept constant during the experiment. Optimal τ values[15] for observation of sum combination harmonics near $2\nu_I$ are determined by $\tau_{opt} = 1/\nu_I(n + 1/2)$ where $n = 0, 1, 2, \ldots$ Therefore, τ values were selected according to this expression in the experiments. The four-pulse ESE envelope depicted in Figure 3 clearly demonstrates the advantage of this sequence by the increase in the echo decay time limited now by the electronic T_1. The decrease of the relaxation decay rate leads to spectral resolution enhancement (Figure 7). The four-pulse ESEEM spectra of the $4VO^{2+}/4Cd^{2+}$ enzyme for the $g_{||}$ components at 2960 and 4250 G contain, in addition to the broad line around the proton Zeeman frequency ν_I, three well-resolved lines in the region of the proton $2\nu_I$. One of them appears exactly at the $2\nu_I$ position and represents the matrix protons. The other peaks shifted by 0.21 and 0.53 MHz and 0.16 and 0.35 MHz (±0.02 MHz) to higher frequencies relative to $2\nu_I$ at the fields 2960 and 4250 G, respectively, arise from two types of protons belonging to ligands. In contrast, spectra recorded at all other magnetic fields between 2960 and 4250 G resolve only one shifted line as seen from Figure 7. Two examples from the central part of the EPR spectrum are obtained on the $g_\perp$ lines at 3400 and 3570 G. The shift observed in these spectra (0.17−0.19 MHz) corresponds to the smaller shift found at the $g_{||}$ components and can be attributed to the same proton. All our attempts to detect well-resolved lines with a larger shift in the middle part of the EPR spectrum were not successful.

At small values of isotropic and anisotropic proton couplings relative to the Zeeman frequency $\nu_I > a/2$ and $T_\perp/2$ (this assumption is valid for oxovanadium complexes), the shift of the maxima of sum combinations from $2\nu_I$ for $g_{||}$ and $g_\perp$ components of the EPR spectrum is determined by the following relations, respectively:[24]

$$\Delta_{||} = (9T_\perp^2 \sin^2\theta_{||} \cos^2\theta_{||})/4\nu_I \qquad (2)$$

$$\Delta_\perp = \begin{cases} (9T_\perp^2 \sin^2\theta_{||} \cos^2\theta_{||})/4\nu_I & \text{for } \theta_{||} \le 45° \text{ or } \theta_{||} \ge 135° \\ 9T_\perp^2/16\nu_I & \text{for } 45° \le \theta_{||} \le 135° \end{cases}$$

Here, $\theta_{||}$ is the angle between the principal directions of the axial proton hfi tensor and the **g** tensor of the complex.

Since the measured shifts depend on the value of the applied magnetic field, it is more convenient to use the parameter $\Delta_{eff} = 2/3(\Delta_{exp}\nu_I)^{1/2}$ which is determined in each case only by hyperfine parameters (geometrical position) of the contributing proton. The values of Δ_{eff} for the shifted proton sum combination in the middle area of the EPR spectrum including $g_\perp$ and the extra adsorption components do not differ within experimental accuracy from $\Delta_{eff} = 1.1 \pm 0.03$ MHz for the line with the smaller shift at the $g_{||}$ components. This might be taken to indicate that our experiments do not give effective orientational selection and the spectra reported correspond well to the completely orientationally-disordered case when $\Delta = 9T_\perp^2/16\nu_I$ or $\Delta_{eff} = |T_\perp|/2$. However, all results previously published for oxovanadium complexes, together with the pronounced orientational dependence of the nitrogen ESEEM discussed above, and even the behavior of the second line with the larger shift in the proton four-pulse spectra contradict this possibility. Therefore, the second explanation is that $\theta_{||} \simeq 45°$ or 135° for the proton with the smaller shift. At this angle the shift on $g_{||}$ and $g_\perp$ components is determined by the same expression as for the orientationally-disordered system. With this provision one can find $|T_\perp| = 2.2 \pm 0.06$ MHz, which corresponds to a distance of 3.3 ± 0.03 Å for the proton from the paramagnetic ion in the point-dipole approximation. Simulations of proton four-

Table 2. Nitrogen Hyperfine and Quadrupole Couplings Obtained by ENDOR and ESEEM Spectroscopies in Model Vanadyl Complexes and in Vanadyl-Substituted Proteins

complex/protein	ENDOR	ESEEM
$VO^{2+}(acac)_2$–pyridine	$A_{\|\|}^N = 6.5$ MHz, $Q_{\|\|}^N = 0.85$ MHz (Kirste and van Willigen[26])	$A_{\|\|}^N = 6.0$ MHz, $A_\perp^N = 5.6$ MHz (Astashkin et al.[6])
VO^{2+}–(imidazole)$_4$	$A_{\|\|}^N = 7.40$ MHz, $A_{\|\|}^N = 0.23$ MHz (N1) $A_{\|\|}^N = 6.64$ MHz, $Q_{\|\|}^N = 0.80$ MHz (N3) (Mulks et al.[27])	$A_{\|\|}^N = 0.3$ MHz (N1) (Dikanov et al.[29])
VO^{2+}–(histidine)$_n$	$A_{\|\|}^N = 6.00$ MHz, $Q_{\|\|}^N = 0.76$ MHz (Mulks et al.[27])	
VO^{2+}–apoferritin	$A_{\|\|}^N = 7.14$ MHz, $Q_{\|\|}^N = 0.24$ MHz (N1) $A_{\|\|}^N = 6.36$ MHz, $Q_{\|\|}^N = 0.84$ MHz (N3) (Hanna et al.[28])	$A_{\|\|}^N = 7.1$ MHz, $A_\perp^N = 6.6$ MHz (Gerfen et al.[13])
VO^{2+}–transferrin	$A_{\|\|}^N \sim 7.4$ MHz (Hanna et al.[28])	$a = 6.6$ MHz,[a] $a = 7.0$ MHz[b] (Eaton et al.[11])
VO^{2+}–lactoferrin		$a = 6.6$ MHz,[c] $a = 7.0$ MHz[d] (Eaton et al.[11])
$VO^{2+}(hfac)_2$–pyridine[e]		$a = 7.1$ MHz
$VO^{2+}(hfac)_2$–imidazole		$a = 7.6$ MHz (Eaton et al.[11])
$VO^{2+}(meox)_2$[f]		$A_{\|\|}^N = 6.4$ MHz, $Q_{\|\|}^N = 0.6$ MHz, $A_x^N = 6.1$ MHz, $A_y^N = 5.6$ MHz
$VO^{2+}(mim)_4Cl^+$ [g]		$A_{\|\|}^N = 6.35$ MHz, $Q_{\|\|}^N = 0.8$ MHz, $A_x^N = 6.94$ MHz, $A_y^N = 6.00$ MHz (Reijerse et al.[7])
VO^{2+}–XylI	$A_{\|\|}^N = 13.2$ MHz (Bogumil et al.[4])	$A_{\|\|}^N = 5.7$ MHz, $Q_{\|\|}^N = 0.64$ MHz (Dikanov et al., this work)

[a] TF–CO_3. [b] TF–ox. [c] Lf–CO_3. [d] Lf–ox. [e] hfac = hexafluoroacetylacetonate. [f] meox = 2-methylquinolin-8-oxolato. [g] mim = 1-methylimidazole.

pulse ESEEM spectra with correlated variations of $T_\perp$ and $\theta_{||}$ according to eq 2 exhibit the best correspondence with experimental changes in the amplitude of the shifted sum combination harmonic relative to the matrix sum combination line at $T_\perp = -2.3$ MHz and $\theta_{||} = 40° \pm 10°$, i.e., at the parameters practically coincident with ones estimated from a simple analysis of the line positions.

Inclusion of the rhombicity of hfi with the vanadium nucleus ($A_y^v - A_x^v = 2$ G) leading to the additional orientational selection of the complexes in the xy plane yields an estimation of the angle $\psi = 45° \pm 10°$ for the orientation of the proton hfi tensor principal axis relative to the A_x^v and A_y^v axes. At the angles $\psi \simeq 0°$ or 90°, the projection of the principal axis direction onto the xy plane is close to one of the axes of the vanadium hfi tensor; the amplitude of sum combination is significantly reduced and cannot be recovered at any reasonable a and $T_\perp$. The same explanation is applicable to the absence of the second proton line in the $g_\perp$ spectra if the corresponding proton angle is assumed to be $\psi \approx 0°$ or 90°. However, it does not lead to a complete diminishing of the line intensity in the calculated spectra.

The other way to decrease the line amplitude is connected with the suppression effect determined by the term[15,17]

$$C_c = \cos[\pi(\nu_\alpha + \nu_\beta)\tau] - \cos[\pi(\nu_\alpha - \nu_\beta)\tau] \qquad (3)$$

for the sum combination in four-pulse ESEEM. For the chosen experimental conditions (see above) the first term in eq 3 is very close to −1. Then hyperfine couplings leading to complete suppression of the line intensity should satisfy the relation $\cos[\pi(\nu_\alpha - \nu_\beta)\tau] \simeq -1$, or $A_\perp^H(\chi) \simeq 1$ assuming $\nu_\alpha - \nu_\beta \simeq A_\perp^H(\chi)$. Since the maximum of the sum combination line corresponds to the orientation when the magnetic field and the unique axis of the proton hfi tensor form an angle of about 45° (for $\nu_I > a, T_\perp$), one can obtain $A_\perp^H(\chi) = a - T_\perp/2$. As a result, the following limitation is derived for $\tau = 232$ ns: $|a - T_\perp/2| \simeq 4$ MHz. An additional demand on the anisotropic hfi of this proton $T_\perp^2 \cos^2\theta_{||} \sin^2\theta_{||} = 2.7$ MHz follows from the position of the second shifted line in $g_{||}$ spectra, which leads to the inequality $|T_\perp| \geq 3.3$ MHz. It means that for the reasonable values $3.3 \leq |T_\perp| \leq 6$ MHz the suppression of the sum combination in $g_\perp$ spectra requires noticeable isotropic hfi for the corresponding proton. This is characteristic of the protons located near the equatorial plane in vanadyl complexes.[25] Using the information delineated, we were able to reproduce completely the experimental behavior of sum combinations in $g_{||}$ and $g_\perp$ spectra at different fields (Figure 7) with the set of parameters for the first ($T_\perp = -2.3 \pm 0.1$ MHz, $a = 0$, $\theta_{||} = 40° \pm 10°$ or $140° \pm 10°$, $\psi = 35° \pm 10°$) and second ($T_\perp = -3.6 \pm 0.1$ MHz, $a = 1.8 \pm 0.3$ MHz, $\theta_{||} = 60° \pm 5°$ or $120° \pm 5°$, $\psi = 0° \pm 10°$) protons. The corresponding distances in the point-dipole approximation are 3.25 and 2.8 Å, respectively.

Discussion

The ESEEM spectra of VO^{2+}-substituted D-xylose isomerase confirm the existence of a nitrogen ligand in the high-affinity binding site. Analysis with previous approaches gave an almost isotropic nitrogen hyperfine coupling of $A^N \simeq 6$ MHz. The simulations of ESEEM spectra for selected $g_{||}$ and $g_\perp$ orientations with a second-order treatment led only to a slight correction of this value. Table 2 summarizes the published data on nitrogen ligand characterization of VO^{2+}–proteins and VO^{2+}–(imidazole/histidine) models. All previous publications report a mainly isotropic hyperfine coupling of $A^N \simeq 6$–7 MHz in these complexes from the equatorially coordinated imine nitrogen (N3) of the imidazole ring. Therefore, it is reasonable to attribute the observed nitrogen ESEEM in XylI also to the equatorially coordinated imine nitrogen of the histidine residue. This

(25) Atherton, N. M.; Shackleton, J. F. *Mol. Phys.* **1980**, *39*, 1471.
(26) Kirste, B.; van Willigen, H. *J. Phys. Chem.* **1982**, *86*, 2743.
(27) Mulks, C. F.; Kirste, B.; van Willigen, H. *J. Am. Chem. Soc.* **1982**, *104*, 5906.
(28) Hanna, P. M.; Chasteen, N. D.; Rottman, G. A.; Aisen, P. A. *Biochemistry* **1991**, *30*, 9210.

assignment is confirmed by the recent direct observation[29] of the interaction with the remote, amine nitrogen (N1) in VO^{2+}–([^{15}N]imidazole)$_4$ with a significantly smaller coupling of $A^N \simeq 0.3$ MHz (for ^{14}N).

The nitrogen isotropic constant $a = 5.65$ MHz greatly exceeds the principal elements of the anisotropic hfi tensor (0.4, ~0, −0.4) MHz. These results are in a good quantitative agreement with recent ESEEM investigation[30] of VO^{2+}–porphyrins where the corresponding hyperfine tensor elements $|a| = 7.2$ MHz and (0.5, 0, −0.5) MHz for pyrrole nitrogens were reported. Estimations performed in ref 30 reasonably explain such parameters by indirect spin transfer plus dipole–dipole coupling. This involves transfer of spin densities $\varrho_s \simeq (4-5) \times 10^{-3}$ and $\varrho_p \simeq (3-4) \times 10^{-3}$ on the 2s and 2p nitrogen orbitals, respectively. Under such conditions the anisotropic coupling from the 2p spin density is comparable with the coupling created by the direct dipole–dipole interaction between the unpaired electron on the vanadium 3d orbital ($\varrho_d \simeq 1$) and the nitrogen nucleus at the distance 2.1–2.2 Å. These two contributions to the anisotropic hfi tensor can almost cancel each other, if as expected[30] negative spin densities are formed on the nitrogen 2s and 2p orbitals by the spin-transfer mechanism.

Additional evidence for equatorial coordination by the imine nitrogen comes from consideration of the quadrupole coupling. The parameters $K = 0.5$ MHz and $\eta = 1$ with $K^2(3 + \eta^2) = 1$ MHz^2 correspond well to the estimation of $K^2(3 + \eta^2) = 1.03 \pm 0.12$ MHz^2 derived from the second-order contribution to modulation harmonics. These values differ significantly from the quadrupole couplings reported for imine ($K = 0.81-0.84$ MHz, $\eta = 0.13$, $K^2(3 + \eta^2) = 1.98-2.12$ MHz^2) and amine ($K = 0.35$ MHz, $\eta = 0.915-0.995$, $K^2(3 + \eta^2) = 0.47-0.49$ MHz^2) nitrogens in noncoordinated imidazole and histidine[31] but correspond to the constant $K = 0.47-0.7$ MHz leading to $K^2(3 + \eta^2) \simeq 0.8-1.5$ MHz^2 obtained[32] for the imino nitrogen of imidazole coordinated with Zn^{2+} and Cd^{2+}. In contrast, only slight variations of the quadrupole coupling constant $K = 0.35-0.43$ MHz have been evidenced for the amine nitrogen in Zn^{2+}, Cd^{2+}, and Cu^{2+} complexes with imidazole[32,33] and in Cu^{2+}–proteins.[34]

Additional support for the quadrupole parameters follows from the behavior of the quadrupole tensor of the N3 imidazole nitrogen of histidine in 1-histidine monochloride monohydrate[35] and Cu^{2+}–1-histidine monochloride monohydrate[36] single crystals. Both imidazole nitrogens are protonated in 1-histidine monochloride monohydrate. The N3 nitrogen has a nqi tensor ($K = 0.64$ MHz, $\eta = 0.945$, $K^2(3 + \eta^2) = 1.6$ MHz^2)[35] with the maximal principal direction (−1.287 MHz) normal to the ring plane, and the minimal one (0.033 MHz) aligned along the N–H bond. The nqi tensor of the N3 nitrogen coordinated to the copper in Cu^{2+}–1-histidine monochloride monohydrate is characterized by the values $K = 0.46$ MHz, $\eta = 0.63$, and $K^2(3 + \eta^2) = 0.72$ MHz^2.[36] The copper binding to the N3 nitrogen is accompanied by an interchange of the principal directions of the quadrupole tensor created by a large change in the valence occupancy along the N–Cu bond as compared to the N–H bond.[37] On binding, the maximal principal direction (−0.92 MHz) is in the imidazole plane and aligned with the lone pair sp^2 nitrogen orbital while the minimal one (0.17 MHz) is normal to the plane. However, even with interchange of the principal directions, their misalignment for the N3 nitrogen in these two systems does not exceed 11°.[37] Less misalignment (not more than 4°) for the principal axes of the N1 nitrogen was found from comparison of the NMR measurements of 1-histidine[35] and ESEEM of Cu^{2+}–1-histidine monochloride monohydrate.[37] The copper-coordinated imidazole moiety is not changed significantly as compared to the structure of the molecule in the undoped crystal.[37] The conclusion appears warranted that the nqi tensor principal directions are mainly connected with the imidazole moiety itself and thus can be effectively used to characterize the histidine orientation in the VO^{2+} complex also.

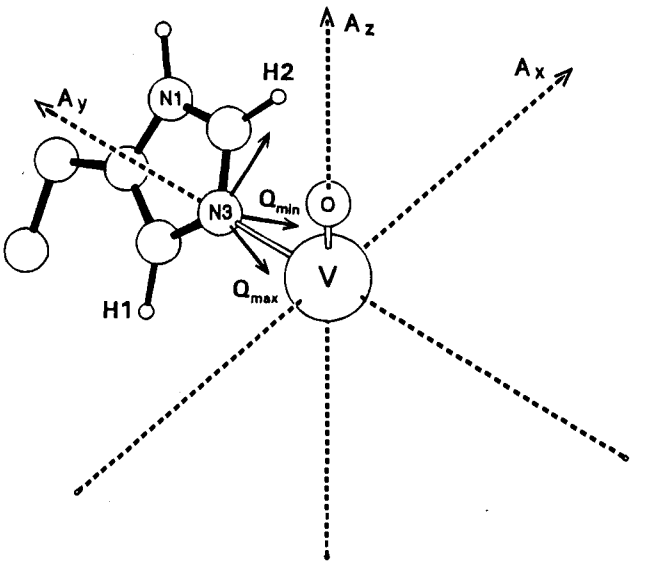

Figure 8. Proposed model of histidine coordination in VO^{2+}–XylI based on the obtained quadrupole tensor of the N3 nitrogen.

If the directions of the nqi tensor principal axes in VO^{2+}–XylI are placed as in Cu^{2+}–1-histidine monochloride monohydrate (i.e., the maximal direction (−1 MHz) is along the lone pair sp^2 nitrogen orbital, and the minimal direction (~0 MHz) is normal to the ring plane), then the Euler angles of the tensor orientation in the frame of the vanadium hfi tensor correspond to equatorial coordination of the N3 nitrogen. According to these angles, the maximal principal axis (or lone pair nitrogen orbital) lies in the xy plane of the complex ($\beta = 90°$) and forms an angle of $|\gamma| = 20°$ with the A_y^V axis. The angle $|\alpha| = 35°$ determines the orientation of two other quadrupole axes or in practice the deviation of the imidazole ring plane from orthogonality to the metal complex plane. Figure 8 demonstrates the expected orientation of the histidine molecule. Note that our Euler angles are in a good agreement with those described by the orientation of the imidazole ring coordinated to Mn^{2+}: $|\alpha| = 20°$, $|\beta| = 94°$, $|\gamma| = 25°$. The latter were calculated on the basis of the X-ray diffraction structure[38] assuming that the VO^{2+} ion occupies the same Mn^{2+}-binding position in site B with the z axis pointed to the sixth water axial

(29) Dikanov, S. A., Burgard, C.; Hüttermann, J. *Chem. Phys. Lett.* **1993**, *212*, 493.
(30) Fukui, K.; Ohya-Nishiguchi, H.; Kamada, H. *J. Phys. Chem.* **1993**, *97*, 1185.
(31) (a) Edmonds, D. T.; Summers, C. P. *J. Magn. Reson.* **1973**, *12*, 134. (b) Hunt, M. J.; Mackay, A. L.; Edmonds, D. T. *Chem. Phys. Lett.* **1975**, *34*, 473. (c) Hunt, M. J.; Mackay, A. L. *J. Magn. Reson.* **1976**, *22*, 295.
(32) Ashby, C. I. H.; Cheng, C. P.; Brown, T. L. *J. Am. Chem. Soc.* **1978**, *100*, 6057.
(33) Mims, W. B.; Peisach, J. *J. Chem. Phys.* **1978**, *69*, 4921.
(34) Jiang, F., McCracken, J., Peisach, J. *J. Am. Chem. Soc.* **1990**, *112*, 9035.
(35) McDowell, C. A.; Naito, A.; Sastry, D. L.; Takegoshi, K. *J. Magn. Reson.* **1986**, *69*, 283.
(36) McDowell, C. A.; Naito, A.; Sastry, D. L.; Cui, Y. U.; Sha, K.; Yu, S. X. *J. Mol. Struct.* **1989**, *195*, 361.
(37) Colaneri, M. J.; Peisach, J. *J. Am. Chem. Soc.* **1992**, *114*, 5335.
(38) Collyer, C. A.; Henrick, K.; Blow, D. M. *J. Mol. Biol.* **1990**, *212*, 211.

ligand. The orientation of the A_y^V axis is suggested to be aligned with the V−N bond.

In this model (Figure 8) the distances from the vanadium nucleus to the nearest protons of the imidazole ring and their orientations relative to the V=O bond (r = 3.47 Å and $\theta_{||}$ = 120° for H_1 and r = 2.95 Å and $\theta_{||}$ = 55° for H_2) correspond to ones obtained from the analysis of the sum combinations to within ~0.2 Å and ~10° (at the expected V−N distance of 2.2 Å as in Mn^{2+}-doped enzyme). One should realize, however, that the nqi results allow restriction only of the *orientation* of the imidazole ring in the vanadium frame, leaving the *position* of the ligand uncertain. In the model in Figure 8 the coordinated imine nitrogen is placed in the equatorial plane of the complex together with the vanadium atom. However, in principle, it can lie above as well as below the equatorial plane. The X-ray diffraction structure[38] indicates a significant deviation of the coordinated nitrogen from the equatorial plane ($\theta_{||} \simeq 72°$) in the Mn^{2+} complex. However, one can accept this angle for VO^{2+} with a large reservation. It is also difficult to obtain the information required from the hfi tensor as quantum-chemical calculations to be necessary for the interpretation of the highly nonaxial tensor of the imine nitrogen. Obviously, this uncertainty can be responsible for the slight discrepancies in the proton location in the model of Figure 8 from those obtained in the ESEEM analysis. Therefore, one can strongly expect the two shifted sum combinations to be associated with the imidazole protons nearest to the coordinated nitrogen. This assignment finds some confirmation in consideration of the angles $\psi = 0° \pm 10°$ and $\psi = 35° \pm 10°$ discovered for the two protons. The difference $\Delta\psi = 35° \pm 20°$ reflects the mutual orientation of the proton hfi principal axes in the xy complex plane. The same angle derived from the nitrogen-based model of Figure 8 appears to be $\Delta\psi = 50°$ and falls well within the experimental interval. Finally, the inspection of the X-ray structure for yet another nearby proton possibly responsible for shifted sum combinations gives less suitable candidates.

Conclusion

The ESEEM study presented here clearly demonstrates the existence of an equatorially coordinated nitrogen from the histidine residue with a hyperfine coupling of $A^N \simeq 6$ MHz in the high-affinity site of VO^{2+}-substituted XylI. This value for the hyperfine coupling is in a good agreement with *all* previously reported values of the nitrogen hyperfine coupling of equatorial ligands obtained by ENDOR and ESEEM in vanadyl proteins and their model complexes. As a consequence, the previous, ENDOR-derived[4] value of $A_{||}^N$ = 13.2 MHz for VO^{2+}−XylI cannot be upheld and the use of this enzyme as an example of axial histidine coordination[14,28] is not supported. Since the earlier value is about twice that obtained here, one can ascribe some ENDOR lines to double-quantum transitions. Work is under way to clarify this discrepancy.

The second result of the present work is the detailed analysis of the nitrogen basic and combination lines in orientationally-selected two-pulse ESEEM (including, for the first time, second-order treatment and complete simulations of $g_{||}$ and $g_\perp$ spectra) which allows the determination of hfi and nqi tensor principal values and directions. As shown here, these data form a reliable basis for the establishment of the detailed geometry of the nitrogen ligation.

The VO^{2+} cation has proven to be a generally useful paramagnetic probe in proteins involving divalent cations (Mg^{2+}, Ca^{2+}, Mn^{2+}) for their catalytic function.[39,40] The investigation performed strongly supports the further application of VO^{2+} as a spin probe in conjunction with ESEEM spectroscopy for the detailed investigation of nitrogen ligands in active metal sites of proteins.

Acknowledgment. S.A.D. acknowledges receipt of the Alexander von Humboldt Foundation Research Fellow Award (06/01/92 to 10/31/93) and the hospitality of the Biophysics Department of Saarland University. This work is part of a program funded by the Deutche Forschungsgemeinschaft. Part of this work was sponsored by the U.S. Department of Energy under Contract No. DE-AC06-76RL0-1830 and by Associated Western Universities, Inc., Northwest Division (AWU NW), under Grant No. DE-FG06-89ER-75522 or DE-FG06-92RL-12451 with the U.S. Department of Energy. The authors are indebted to Dr. M. K. Bowman for the critical reading of the paper and his useful comments.

Appendix

The harmonics which can appear in two-pulse ESEEM, their first-order frequencies, and some additional designations used in the paper are given in eq A1. A_n and Q_n in these expressions

$$\nu_{sq+}^{(1)} = A_n/2 + \nu_I + 3Q_n/2 \quad \nu_{sq+}^{(2)} = A_n/2 + \nu_I - 3Q_n/2 \quad \nu_{qd+} = A_n + 2\nu_I$$

$$\nu_{sq-}^{(1)} = A_n/2 - \nu_I + 3Q_n/2 \quad \nu_{sq-}^{(2)} = A_n/2 - \nu_I - 3Q_n/2 \quad \nu_{qd-} = A_n - 2\nu_I$$

$$\nu_{sq+}^{(1)} + \nu_{sq-}^{(1)} = A_n + 3Q_n \quad \nu_{sq+}^{(2)} + \nu_{sq-}^{(2)} = A_n - 3Q_n \quad \nu_{ss+} = \nu_{sq+}^{(1,2)} + \nu_{sq-}^{(2,1)} = A_n$$

$$\nu_{sq+}^{(1)} - \nu_{sq-}^{(2)} = 2\nu_I + 3Q_n \quad \nu_{sq+}^{(2)} - \nu_{sq-}^{(1)} = 2\nu_I - 3Q_n \quad \nu_{ss-} = \nu_{sq+}^{(1,2)} - \nu_{sq-}^{(1,2)} = 2\nu_I$$

$$\nu_{dq+} + \nu_{sq-}^{(1)} = 3A_n/2 + \nu_I + 3Q_n/2 \quad \nu_{dq-} + \nu_{sq+}^{(1)} = 3A_n/2 - \nu_I + 3Q_n/2$$

$$\nu_{dq+} + \nu_{sq-}^{(2)} = 3A_n/2 + \nu_I - 3Q_n/2 \quad \nu_{dq-} + \nu_{sq+}^{(2)} = 3A_n/2 - \nu_I - 3Q_n/2$$

$$\nu_{dq+} - \nu_{sq-}^{(1)} = A_n/2 + 3\nu_I - 3Q_n/2 \quad \nu_{dq-} - \nu_{sq+}^{(1)} = A_n/2 - 3\nu_I - 3Q_n/2$$

$$\nu_{dq+} - \nu_{sq-}^{(2)} = A_n/2 + 3\nu_I + 3Q_n/2 \quad \nu_{dq-} - \nu_{sq-}^{(1)} = A_n/2 - 3\nu_I - 3Q_n/2$$

$$\nu_{dd+} = \nu_{dq+} + \nu_{dq-} = 2A_n \quad \nu_{dd-} = \nu_{dq+} - \nu_{dq-} = 4\nu_I \quad \text{(A1)}$$

correspond to the hyperfine and quadrupole coupling of a nitrogen ligand nucleus at an arbitrary orientation of the external magnetic field in the coordinate system of the vanadium hfi tensor. For instance, they equal $A_{||}^N$ and $Q_{||}^N$ when the magnetic field is arranged on the $g_{||}$ component of the EPR spectrum.

The contribution of the second-order terms to the modulation harmonics of the ligand ^{14}N with $A \gg \nu_I$, Q is calculated as

$$\nu_{ss+} = \nu_{sq+}^{(1,2)} + \nu_{sq-}^{(2,1)} = A_n + A_n A_n^{(2)}/2(A_n^2/4 - \nu_I^2) \mp \nu_I Q_n^{(2)}/(A_n^2/4 - \nu_I^2)$$

(39) Chasteen, N. D. In *Biological Magnetic Resonance*; Berliner, L. J., Reuben, J., Eds.; Plenum: New York, 1981; p 53.

$$\nu_{sq+}^{(1,2)} = A_n/2 + \nu_I \pm 3Q_n/2 + (A_n^{(2)} \pm Q_n^{(2)})/2(A_n/2 + \nu_I)$$

$$\nu_{sq-}^{(1,2)} = A_n/2 - \nu_I \pm 3Q_n/2 + (A_n^{(2)} \pm Q_n^{(2)})/2(A_n/2 - \nu_I)$$

$$\nu_{dq\pm} = A_n \pm 2\nu_I + A_n^{(2)}/(A_n/2 \pm \nu_I)$$

$$\nu_{dd-} = 4\nu_I - 2\nu_I A_n^{(2)}/(A_n^2/4 - \nu_I^2) \qquad \text{(A2)}$$

where $A_n^{(2)} = B^2/4 + K^2(3 + \eta^2) - 3/4Q_n^2$, $B^2 = T_{nl}^2 + T_{nm}^2$, $Q_n^{(2)} = 3(Q_{nl}T_{nl} + Q_{nm}T_{nm})$, n is the direction of the applied magnetic field, and l and m are arbitrary directions in the plane normal to the magnetic field direction. The second-order expressions for ^{14}N single-quantum frequencies have been previously derived by Scholes et al.[41] for collinear axes of hyperfine and quadrupole tensors when the magnetic field is pointed along the canonical orientations. Our formulas for $\nu_{sq\pm}$ transform to their expression at the indicated limits. Expressions A2 were obtained in the high-field approximation and, therefore, do not contain the term $\sim 1/\nu_e$ considered in ref 41. It is negligible for the nitrogen hyperfine coupling in this complex.

The diagonal elements of the hyperfine tensor of the ligand nucleus in the coordinate system of the rhombic vanadium hyperfine tensor are

$$A_{||}^N = a + T_{11}/2\{[3(1 + s) - (1 - s)\cos 2\phi]\sin^2\theta - 2(1 + s)\} = a + T_{||}$$

$$A_{\perp(1,2)}^N = a - T_{||}/2 \pm R \qquad \text{(A3)}$$

where $R = T_{11}/4\{[3(1 + s)\sin^2\theta + (1 - s)(\cos 2\phi)(1 + \cos^2\theta)]^2 + 4(1 - s)^2\sin^2 2\phi\cos^2\theta\}^{1/2}$, $T_{22}/T_{11} = s$ with $|T_{33}| \geq |T_{11}| \geq |T_{22}|$ assumed, and ϕ, θ, and ψ are the Euler angles which determine the orientation of the ligand nitrogen hfi tensor.

The diagonal elements of the quadrupole tensor of nitrogen in the vanadium coordinate system are given as

$$Q_{||}^N = K[(3 + \eta\cos 2\alpha)\sin^2\beta - 2] \qquad \text{(A4)}$$

$$Q_{\perp(1,2)}^N = -Q_{||}/2 \pm J$$

where $J = K/2\{[3\sin^2\beta - (\eta\cos 2\alpha)(1 + \cos^2\beta)]^2 + 4\eta^2\sin^2 2\alpha\cos^2\beta\}^{1/2}$, $K = e^2qQ/4h$, η is the symmetry parameter, and α, β, and γ are the Euler angles which determine the orientation of the nitrogen quadrupole tensor.

The hyperfine and quadrupole couplings of the ligand nucleus at an arbitrary orientation of the magnetic field determined by the angle χ in the xy plane of the vanadium coordinate system are

$$A_\perp^N(\chi) = a - T_{||} + R\cos(2\psi + 2\chi + 2\chi_o) \qquad \text{(A5)}$$

where $\text{ctg}\, 2\chi_o = [3(1 + s)\sin^2\theta + (1 - s)(\cos 2\phi)(1 + \cos^2\theta)]/(2(1 - s)\sin 2\phi\cos\theta)$ and

$$Q_\perp^N(\chi) = -Q_{||}/2 + J\cos(2\gamma + 2\chi - 2\chi_o) \qquad \text{(A6)}$$

where $\text{ctg}\, 2\chi_o = [3\sin^2\beta - (\eta\cos 2\alpha)(1 + \cos^2\beta)]/(2\eta\sin 2\alpha\cos\beta)$.

JA9439377

(40) Eaton, S. S.; Eaton, G. R. In *Vanadium in Biological Systems*; Chasteen, N. D., Ed.; Kluwer, Publishers: Dordrecht, The Netherlands, 1990; p 199.

(41) Scholes, C. P.; Lapidot, A.; Mascarenhas, R.; Inubushi, T.; Isaakson, R. A.; Feher, G. *J. Am. Chem. Soc.* **1982**, *104*, 2724.